Protein-fluctuation-induced water-pore formation in ion channel voltage-sensor translocation across a lipid bilayer membrane

Suneth P. Rajapaksha, Nibedita Pal, Desheng Zheng, and H. Peter Lu*

Department of Chemistry and Center for Photochemical Sciences, Bowling Green State University, Bowling Green, Ohio 43403, USA

(Received 24 April 2015; published 30 November 2015)

We have applied a combined fluorescence microscopy and single-ion-channel electric current recording approach, correlating with molecular dynamics (MD) simulations, to study the mechanism of voltage-sensor domain translocation across a lipid bilayer. We use the colicin Ia ion channel as a model system, and our experimental and simulation results show the following: (1) The open-close activity of an activated colicin Ia is not necessarily sensitive to the amplitude of the applied cross-membrane voltage when the cross-membrane voltage is around the resting potential of excitable membranes; and (2) there is a significant probability that the activation of colicin Ia occurs by forming a transient and fluctuating water pore of ∼15 Å diameter in the lipid bilayer membrane. The location of the water-pore formation is nonrandom and highly specific, right at the insertion site of colicin Ia charged residues in the lipid bilayer membrane, and the formation is intrinsically associated with the polypeptide conformational fluctuations and solvation dynamics. Our results suggest an interesting mechanistic pathway for voltage-sensitive ion channel activation, and specifically for translocation of charged polypeptide chains across the lipid membrane under a transmembrane electric field: the charged polypeptide domain facilitates the formation of hydrophilic water pore in the membrane and diffuses through the hydrophilic pathway across the membrane; i.e., the charged polypeptide chain can cross a lipid membrane without entering into the hydrophobic core of the lipid membrane but entirely through the aqueous and hydrophilic environment to achieve a cross-membrane translocation. This mechanism sheds light on the intensive and fundamental debate on how a hydrophilic and charged peptide domain diffuses across the biologically inaccessible high-energy barrier of the hydrophobic core of a lipid bilayer: The peptide domain does not need to cross the hydrophobic core to move across a lipid bilayer.

DOI: 10.1103/PhysRevE.92.052719 PACS number(s): 82.39.−k

I. INTRODUCTION

Ion channels are membrane proteins capable of regulating the ion flow across cell membranes. The channels are responsive to specific stimuli, for example, cross-membrane voltage change, ligand binding, local chemical composition change, mechanical stress, or light absorption [1–7]. Polypeptide domains with high charge densities, known as voltage-sensitive peptides, are generally involved in voltage-gated ion channel activities. Typically, the conformational changes of a charged polypeptide domain under a transmembrane voltage play critical roles in the voltage-gated ion channel open-close activations [8–10]. In recent years, there has been an intensive debate on the mechanism and dynamics of moving a charged peptide chain across a lipid membrane. It has been estimated that the energy cost of pulling a charged peptide chain into the hydrophobic core of a lipid membrane is likely too high to occur under physiological conditions. For example, the free energy cost to insert an arginine residue into the hydrophobic core of a lipid bilayer is estimated to be as high as 17 kcal/mole [11], and that for a voltage-sensor polypeptide domain can be as high as 265 kcal/mol [12]. On the other hand, the experimentally measured energy barrier for inserting a voltage-sensor polypeptide is only ∼2.5 kcal/mole [13]. The apparent discrepancy between the theoretical prediction and experimental finding compelled us to look for a deeper mechanistic understanding of the voltage-sensor domain insertion and translocation across the lipid membrane. The fundamental question here concerns the dynamics and mechanism through which a charged peptide domain moves across the hydrophobic core of a lipid membrane under a transmembrane electric field. Consequently, it can shed lights on some of the other fundamental questions such as how to block a voltage-gated ion channel when it becomes permeable as a result of mutations [14].

In this paper we present a detailed study on the colicin Ia channel unraveling an additional mechanism of voltage-sensor domain diffusion through the hydrophobic core of a lipid bilayer. Although it was previously reported that the peptide translocation across the membrane can occur by forming a pore in the lipid membrane [14,15], there is a lack of comprehensive understanding about the mechanism involved in the process. Our results help to understand the mechanistic pathway of how a charged polypeptide chain can diffuse across the lipid membrane at low cost of activation barrier energy, much lower than the theoretically estimated energy of pulling a charged peptide into the hydrophobic core region of the membrane. Intrinsically, peptide solvation dynamics plays a critical role in charged polypeptide chain translocation through the membrane as it is a well-established fact that the local solvation dynamics has a crucial role in maintaining the protein's structure-function-dynamics relationship as well as conformational changes during folding and unfolding processes [16–18].

Here, we specifically study the voltage dependency of open-close activity of the colicin Ia ion channel and the translocation mechanism of the α-helices 2–5 of the C domain of colicin Ia across the membrane. We have developed and applied combined study of single-ion-channel electric current recording, fluorescence microscopic imaging, and molecular dynamics (MD) simulations in this work. Colicin Ia is a

*Corresponding author: hplu@bgsu.edu

monomeric-polypeptide with a single voltage-sensor domain. Due to its simplicity, we chose the colicin Ia ion channel as the model system for our comprehensive study. Our experimental and computational results suggest that the conformational fluctuations of the colicin Ia under the transmembrane voltage can induce the formation of a hydrophilic water pore across the membrane. The position of the water-pore is nonrandom but right at the insertion site of colicin Ia in the membrane, and the charged polypeptide domain moves across the membrane through the hydrophilic water-pore without entering the hydrophobic core region in the process of the ion channel activation. Ultimately, our study provides a molecular-level answer to a critical question: what is the mechanism by which a large charged peptide domain translocates from the external hydrophilic side of a membrane through the hydrophobic membrane core to the other hydrophilic side of the membrane? The answer to this question presumably has a significant implication in understanding the molecular mechanism of a range of voltage-gated ion channel functions and dynamics [7,19–21].

A. Using colicin Ia in a lipid membrane as the model system to study voltage-sensor domain translocation

Colicin Ia, a water-soluble single-subunit 69 kDa protein of 626 amino acids, is produced by *Escherichia coli* bacteria [22–26] and only a single protein is needed to form an ion channel across a lipid bilayer membrane [27]. Colicin Ia has three main domains performing different functions [Fig. 1(a)]: the T domain, close to the N terminal, translocates the protein across the outer cell membrane; the R domain in the center binds to a receptor in the outer membrane; and the C domain of ∼175 amino acids forms a voltage-gated ion channel in the inner membrane [6,23–25,28]. These three domains are separated from each other by two long α-helices [Fig. 1(a)] [25]. The main function of the protein is carried out by the C domain [blue in Fig. 1(a)] which forms the ion channel in the cell membrane [24,26,29,30]. The α-helices 8 and 9 in the C domain mostly contain uncharged amino acids forming a hydrophobic hairpin [red in Fig. 1(b)] to embed in the hydrophobic core of the membrane, thereby anchoring the C domain [31,32], which is the initial step of the ion channel formation [33]. To form a functional ion channel under a transmembrane electric voltage, the α-helices 2–5 [green in Fig. 1(b)] with a high density of the positively-charged amino acid moves across the cell membrane to bring the helix 1 and helices 6- and 7 into the membrane to join with the membrane-inserted helices 8 and 9 and form an active four-subunit ion channel [Fig. 1(c)] [6,33]. Although the translocation of helices 2–5 for the formation and activation of the ion channel is experimentally proved [6], the mechanism and dynamics of the translocation and channel's open-close activity are yet to be definitively characterized. Further exploration will ultimately lead us to a general understanding of the voltage-sensitive ion channel activation and open-close activity [34,35].

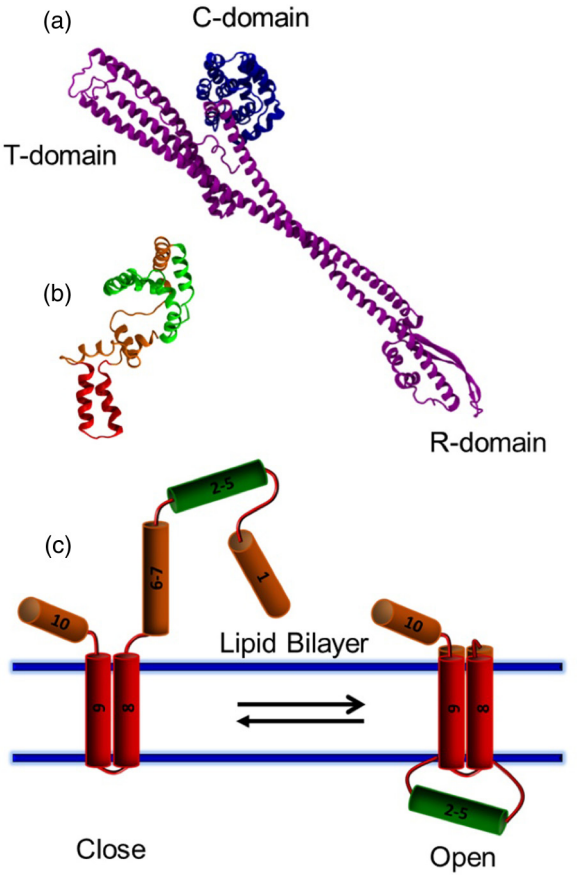

FIG. 1. (Color online) The structure of colicin Ia. (a) Colicin Ia protein. The channel-forming C domain is colored in blue and the rest of the protein is colored in purple. (b) The unwound C domain of colicin Ia. Hydrophobic helices 8 and 9 are shown in red. The membrane-crossing helices 2–5 are shown in green, and the other helices are shown in orange. The net charge of α-helices 2–5 is +7. (c) The open and closed states of the ion channel; the channel activation is related to the translocation of the α-helices 2–5 across the lipid bilayer, which leads the colicin Ia to form the ion channels under a transmembrane voltage.

II. MATERIALS AND METHODS

A. Materials

1,2-diphytanoyl-*sn*-glycero-3-phosphocholine (DPhPC) (Avanti Polar Lipids Inc., Alabama, USA) was used to prepare artificial lipid bilayers. KCl, NaOH, HCl, $CaCl_2$, *n*-decane, 4-(2-hydroxyethyl)-1-piperazine ethanesulfonic acid (HEPES) (Aldrich) and Fluo 8H (AAT Bioquest) were used as received. The colicin Ia used in our experiments was purified, mutated, fluorescein-labeled, and biotinylated by Professor A. Finkelstein's co-workers at the Albert Einstein College of Medicine, NewYork, and has only the C domain (the term "colicin Ia" in the Materials and Methods, and the Results and Discussion sections refers to the C domain of colicin Ia). It has been reported earlier that the biotinylation of colicin Ia does not change its voltage gating characteristics [6], and it is most likely that the fluorescein labeling also does not change significantly the gating mechanism and dynamics of colicin Ia.

B. Single-ion-channel current recording

We prepared a horizontally suspended ∼100 μm diameter DPhPC lipid bilayer to record single ion-channel voltage-clamp current traces and correlated fluorescence imaging. A

detailed description of the bilayer preparation is published elsewhere [36]. Briefly, a horizontally suspended lipid bilayer was prepared at a ~100 μm diameter pinhole pathway by painting 10–20 mg/ml n-decane solution of DPhPC in an electrolyte solution of 1 M KCl, 1 mM ethylene diamine tetra-acetic acid (EDTA), 5 mM $CaCl_2$, and 20 mM HEPES buffer of $pH = 8$ [23]. After the insertion of colicin to the membrane, the single-ion-channel current was recorded with a patch clamp amplifier (EPC7 *plus*, HEKA Electronik, Germany) filtered at 1 kHz. The data were recorded using an LIH 1600 acquisition interface and PULSE V8.80 software (HEKA Electronik, Germany). IGOR PRO (WaveMetrics, Inc.) and MATLAB (MathWorks, Inc.) were used for the data analysis.

C. Single-ion-channel calcium flux fluorescence imaging

We used an established procedure to achieve the calcium flux fluorescence imaging by adding 0.1 M of the Ca^{2+} sensing dye [37] Fluo 8H to the cis side of the lipid bilayer, and adding 1 M Ca^{2+} solution to the trans side of the lipid bilayer. The electrolyte used in this experiment does not contain any Ca^{2+}. The Fluo 8H dye molecules in the cis side emit fluorescence only after binding with Ca^{2+}. The lipid bilayer was illuminated with a 488 nm laser beam (argon ion laser, Melles Griot) in a wide-field epifluorecence imaging configuration [36–39]. The fluorescence signals were collected with an inverted microscope (Axiovert 200M, Zeiss) through a 60× water immersion objective [numerical aperture (NA) of 1.20]. The collected photon signals from the sample were filtered with an HQ505LP filter (Chroma Technology) and recorded with an electron-multiplying charge-coupled device (EMCCD) camera (Princeton Instruments, ProEM 512B).

D. Molecular dynamics simulation

We used the GROMACS V4.5.5 package [40] to perform MD simulations with the extended united-atom version of the GROMOS96 force field [41–45]. The membrane DPhPC bilayer model system and the modified parameters for lipids were used in our MD simulation [46–48]. Before inserting peptide, the only solvated DPhPC bilayer is simulated for 10 ns in an *NPT* (constant number of particles, pressure, and temperature) ensemble. The crystal structure of colicin Ia was downloaded from the Protein Data Bank (PDB ID: 1CII) and edited to contain only the C domain from the 452 residue to the 626 residue based on our examined molecules. Some of the single bonds in the loops of C domain were rotated several degrees until we obtained a reasonable umbrella structure [Fig. 1(b)]. After each rotation, the new structure was inspected to confirm that there were no conflicts between the coordinates of the atoms. All energy minimization used fewer than 1000 steps of the steepest decent method to remove any steric conflicts of the atoms. The helices 8 and 9 of the C domain [red color segments in Fig. 1(b)] were embedded in the lipid bilayer by using the INFLATEGRO algorithm [49]. Then the system was solvated with 36 742 simple point charge waters and NaCl was added to the system at 0.1 M concentration [50]. Energy minimization was achieved by using fewer than 1000 steps of the steepest-decent method to remove any steric conflicts of the atoms. After energy minimization, the system is slowly annealed in an *NPT* ensemble over 500 ps and then equilibrated for another 500 ps in *NPT*. We used a Nosé-Hoover thermostat at 323 K for annealing, equilibration, and the rest of the simulation [51,52]. The MD simulation was performed at a constant temperature, constant pressure, and constant number of molecules. The Parrinello-Rahman algorithm was used to couple the pressure at 1 bar throughout the simulation box [53,54] and the bonds were restrained using the LINCS algorithm [55]. The long-range electrostatic interactions were calculated using the particle mesh Ewald method with a 1.2 nm cutoff for the real space calculations [56]. An electric field with appropriate strength correlating with the experimental conditions was applied in the reverse z direction. The integration time step was 2 fs, and the velocities and coordinates of each atom were saved every 2 ps. The simulation was performed at Ohio Supercomputer Center, using four nodes with ten processors per node. Molecular graphics were developed with Visual Molecular Dynamics (VMD) [57].

E. Combined fluorescence imaging, single-channel electric recording, and MD simulation approach

Combined single-ion-channel electric current recording and fluorescence microscopic imaging are capable of characterizing the mechanism and dynamics of ion-permeable pore formation, cellular response, ion channel functions, and related conformational changes [37,39,58–61]. Furthermore, MD simulations play a complementary role in achieving a molecular-level analysis of ion channel formation and activity dynamics [62–68]. In recent years, theoretical calculation and MD simulation have been extensively applied to study biological membranes, membrane-associated protein dynamics, and biomolecular recognition [49,69–73]. For example, the MD simulation studies of the insertion of α-helices into the membrane and the stability of α-helices in the membrane have been reported [74–77]. Although these studies have provided insightful information about the specific or generalized ion channels, the details of colicin Ia apparently have not been studied with MD simulations, largely due to the lack of experimental structural and dynamic information of the ion channel's membrane-bound states [78]. Nevertheless, in this work, we compared simulation results to the experimental findings to develop a molecular-level picture of peptide translocation across a lipid membrane while forming an active ion channel.

III. RESULTS AND DISCUSSION

A. Understanding the ion channel open-close activity dynamics and mechanism: Activated ion channel open-close state dynamics is primarily driven by stochastic thermal fluctuations of the ion channel's peptide conformations in the membrane

We recorded the single-ion-channel current and conductance fluctuations of colicin Ia channel gating at three different transmembrane voltages; 50, 70, and 100 mV [Figs. 2(a1), 2(a2), and 2(a3), respectively]. The The single ion-channel conductance trajectories clearly show the ion channel closed state at the lower level and open state at the higher level. The ion channel open and closed states are identified by using a threshold value based on the lowest populated conductance in

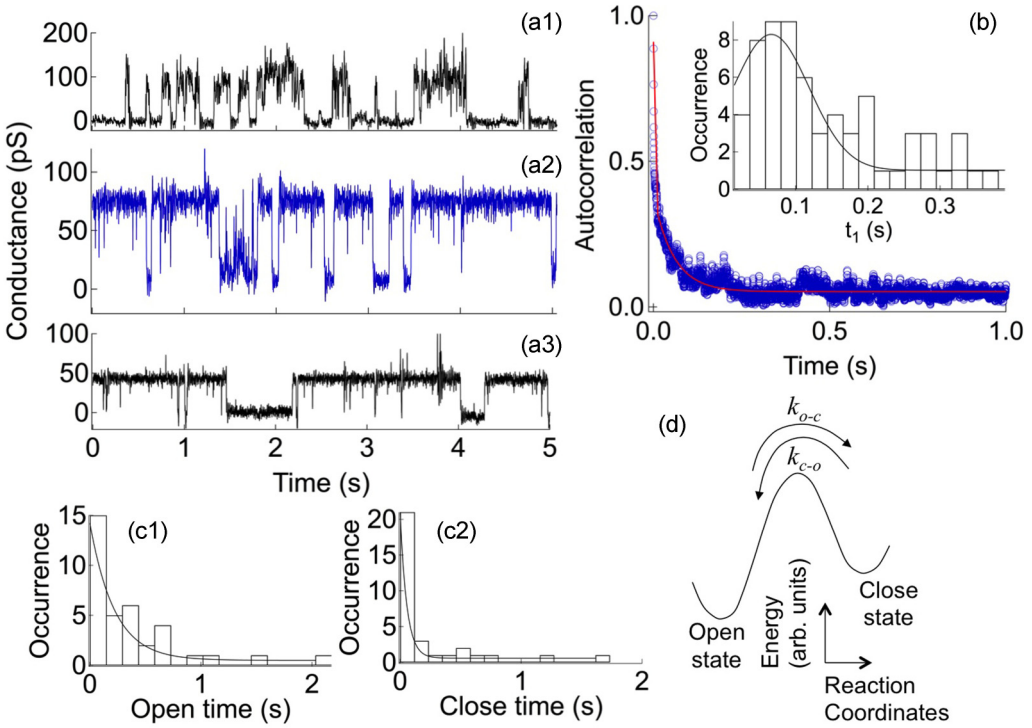

FIG. 2. (Color online) The single-ion-channel conductance trajectories and analysis. (a) The 5-s-long conductance trajectories at (a1) 50 mV (a2) 70 mV and (a3) 100 mV. (b) The autocorrelation function analysis of the conductance trajectory under 70 mV transmembrane voltage. The biexponential decay fitting is shown in red. The faster time component of the decay is 0.093 s. Inset: The distribution of the faster time component (t_1) of the autocorrelation function decay fitting is based on 59 trajectories recorded at 70 mV. The mean of the Gaussian fitting is 0.066 ± 0.018 s. (c1) The distribution of the channel open times with mean at 0.23 ± 0.05 s at 70 mV. (c2) The distribution of the channel close times with mean at 0.043 ± 0.005 s of a 20 s long conductance trajectory at 70 mV. (d) The potential energy surface diagram of the colicin Ia ion channel. k_{o-c} is the transition rate of open to closed and k_{c-o} is the transition rate of closed to open.

the conductance distribution. A state with conductance value higher than the threshold is considered to be the open state, and a state with conductance value lower than the threshold is considered to be the closed state.

We have analyzed the ion channel open-close activity dynamics by calculating the autocorrelation function from the recorded single-ion-channel conductance time trajectories [37,38].

$$C_{\text{auto}}(t) = \langle \Delta A(0) \Delta A(t) \rangle / \langle \Delta A(0)^2 \rangle$$
$$= \langle [A(0) - \langle A \rangle][A(t) - \langle A \rangle] \rangle / \langle [A(0) - \langle A \rangle]^2 \rangle,$$

where $A(t)$ are the signal variables, the conductance, measured from a single ion channel. $\langle A \rangle$ is the mean conductance of the fluctuation trajectory. Figures 2(b), 2(c1), and 2(c2) show the autocorrelation analysis of the conductance trajectories recorded at 70 mV. The recorded continuous conductance trajectories are divided into 5 s segments [Fig. 2(a)], and the autocorrelation function of each trajectory is calculated and the decay time is analyzed [Fig. 2(b)]. The autocorrelations of the conductance follow biexponential decay dynamics essentially due to complex interaction of the ion channel helices with themselves and surrounding local environment that ultimately produce slower and faster time components. The temporal distribution of the slower time component is considerably broad, from milliseconds to seconds, possibly involving some stochastic dynamics of the protein. Furthermore, the narrow faster time distribution gives the mean ($\langle \tau_{o \leftrightarrow c} \rangle$) at 0.066 ± 0.018 s [Fig. 2(b) inset). $\tau_{o \leftrightarrow c}$ is the total time needed for a single event of the channel's open-close transition. The inverse of $\langle \tau_{o \leftrightarrow c} \rangle$ is the rate for the open-close transition ($K_{o \leftrightarrow c}$) and equal to the sum of the channel's open to close rate ($k_{o-c} = 1/\tau_o$) and close to open rate ($k_{c-o} = 1/\tau_c$) [79]:

$$K_{\text{o} \leftrightarrow \text{c}} = k_{o-c} + k_{c-o}. \quad (1)$$

The dwell times of the channel in the open state (τ_o) and the closed state (τ_c) are calculated by using 20 s long conductance trajectories. Using the threshold as we have discussed above, we are able to read out the dwell times of the open and closed states from each single-ion-channel conductance trajectory. Figures 2(c1) and 2(c2) show the distribution of the readout open dwell times and closed dwell times, respectively, and the distribution shows the typical Poisson temporal distribution feature of exponential decays. We separately calculated the average open dwell time ($\langle \tau_o \rangle$) and average closed dwell time ($\langle \tau_c \rangle$) and further calculated the ratio of $\langle \tau_o \rangle / \langle \tau_c \rangle$. The inverses of these dwell times are the average rate of open to closed transition ($1/\langle \tau_o \rangle = \langle k_{o-c} \rangle$) and average rate of close to open transition ($1/\langle \tau_c \rangle = \langle k_{c-o} \rangle$) [Fig. 2(d)] [80]. We have the $\langle k_{o-c} \rangle / \langle k_{c-o} \rangle$ ratio to be 0.194. Since the total rate ($1/\langle \tau_{o \leftrightarrow c} \rangle = K_{o \leftrightarrow c}$) is 15.2 s^{-1}, we calculate k_{o-c} and k_{c-o} to be 2.47 and 12.7 s^{-1}, respectively. The same calculation procedure is followed for the conductance trajectories recorded at 50 and 100 mV transmembrane voltages. At 50 mV, k_{o-c} and

k_{c-o} are 3.17 s^{-1} and 9.66 s^{-1}, respectively, and at 100 mV, k_{o-c} is 2.14 s^{-1} and k_{c-o} is 7.83 s^{-1} (see Ref. [81]).

We observed that the transmembrane voltage is a basic requirement for the starting of the channel open-close activity. Our results show that the most active ion channel is formed with +70 mV electric field, which is near the resting potential of typical excitable cell membranes. In the presence of an external voltage across the membrane, the helices 2–5 in the cis side of the bilayer can drift through the lipid membrane, allowing the protein to form an activated ion channel. However, after the ion channel is formed and activated, the open-close activity is likely to have less dependency on the applied electric field. The rate from open to closed is slightly decreasing with increasing voltage while the rate of closed to open maximizes at +70 mV transmembrane voltage. We attribute this to the fact that at +70 mV, the resting potential of the excitable membranes, the force applied on the helices 2–5 segment is the optimal force to keep the voltage-sensitive segment of the protein at the position in the trans side of the membrane to form the activated ion channel. Lower or higher than +70 mV voltage does not necessarily provide the range of external force needed for helices 2–5 to undergo conformational change in order to form an effective ion channel. The rates of open to close and close to open processes are approximately in the same range, implying that the protein has less dependency on the applied transmembrane voltage for its open-close activity. We suggest that, after the channel is formed in the membrane, the ion channel open-close activity is essentially driven by thermally driven conformational fluctuations of the ion channel and its local membrane environment. As suggested in the literature [82–85], the protein conformational changes or protein folding such as the open-close transition of the ion channels can be a non-Arrhenius process which has a considerably lower activation barrier energy, 2.8-3.1 kcal/mole, than the 13.4-16.0 kcal/mole calculated by using the Arrhenius relationship at the same ambient temperature, assuming the preexponential factor to be 10^{11} to 10^{13} s^{-1}, respectively [82–85]. However, the exact quantitative correlation between thermally driven conformational fluctuations and the electric current on-off changes demands further structural studies, which are beyond the scope of this work. After the formation of the ion channel, the existing transmembrane voltage mostly serves as a biased field to keep helices 2–5 in the trans side, rather than driving the channel open-close conformational motions. The only voltage-dependent process in the colicin Ia ion channel formation involves the translocation of the α-helices 2–5 across the membrane, bringing the α-helices 1, 6, and 7 into the membrane to join with helices 8 and 9 to form the channel configuration, and keeping the translocated helices 2–5 in the trans side of the membrane.

B. Identifying ion channel activation dynamics and mechanism: revealing an additional pathway of voltage-sensor-domain peptide translocation across a lipid bilayer membrane

Based on our experimental results and the above discussion, we attribute the translocation of helices across the membrane to happen only at the activation onset time in a single-channel open-close time trajectory. Nevertheless, the question still remains: how does a large and charged polypeptide domain move across the lipid bilayer from one hydrophilic side through a hydrophobic inner layer to the other hydrophilic side of the membrane to form an activated colicin Ia channel? The answer to this question may provide additional understanding of the molecular mechanism of voltage-gated ion channel functions and dynamics [7,19–21].

The recorded conductance trajectories of a single colicin Ia channel [Fig. 3(a)] clearly show the channel closed state at a lower conductance level and the channel open state at a higher conductance level in the presence of a transmembrane electric field. The average conductance of the single channel is 70 ± 1.9 pS [Fig. 3(b)], consistent with the reported conductance of a typical single colicin Ia ion channel [24].

It is intriguing that the colicin Ia ion channel open-close activity starts with a transient high-conductance signal (THC) [Fig. 3(a)]. The occurrence of the THC state is temporally nonrandom and highly correlated with the onset of the channel open-close activity, i.e., the channel activation onset events. We have observed that the probability of THC state occurrence is about $40\% \pm 10\%$ among our recorded single-ion-channel conductance trajectories when individual active colicin ion channels are formed, i.e., there is a strong temporal correlation between the THC state appearance events and the onset of the single-ion-channel open-close activities. The THC state appears likely to be a precursor event associated with the colicin channel activation. In our experiments, the conductance trajectories of the colicin Ia are recorded under a constant voltage without amplitude and polarity changes, i.e., the transmembrane voltage is applied long before the appearance of the THC state. Therefore, the transient THC signal cannot result from polarization and depolarization or charging and discharging of the lipid bilayer, namely, the typical Faraday charging effect. Furthermore, our data also show that the dynamics of the THC state appearance typically involves multiple steps and significant fluctuations [Fig. 3(c)]. Presumably, the channel open-close activity starts with the formation of the ion channel, and the channel formation is related to the translocation of the α-helices 2–5 across the lipid bilayer under the transmembrane voltage of +70 mV [Fig. 1(c)] [6,23]. We attribute the origin of the transient THC state to the formation of a larger water pore through which the helices 2–5 diffuse across the membrane to form a colicin Ia ion channel in the lipid bilayer.

The mean of the conductance distribution of the THC states is 310 ± 13 pS [Figs. 3(b) and 3(d)]. Assuming the conductivity (σ) and the thickness of the lipid bilayer membrane (l) are constants for a given system during the time of the measurements, the conductance (G) depends only on the size (cross section area A) of the pore pathway, as $G = \sigma A/l$. Therefore, we estimate that the average cross sectional area of the THC pore pathway is about 4.5 times larger than the cross-sectional area of a regular open colicin channel. According to the previously reported channel structure, the channel is hourglass shaped, with an ~18 Å diameter entrance in the cis side, an ~10 Å diameter entrance in the trans side and an ~7 Å diameter narrowing between the entrances [86]. Considering the ~7 Å limiting diameter of the channel, the average cross-sectional area of the THC pore is calculated to be 170.5 $Å^2$ [6], and the diameter is ~ 15 Å. Based on the data of a large number of recorded single-ion-channel activation

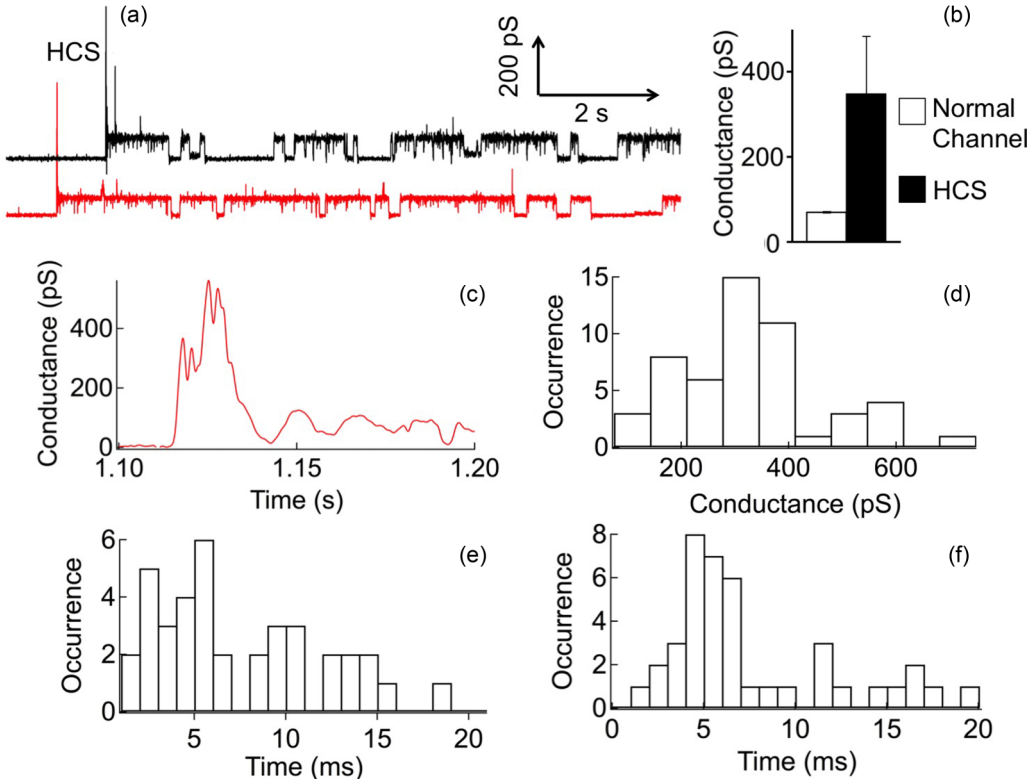

FIG. 3. (Color online) High-conductance-trajectory analysis. (a) Conductance trajectories of single channels. Both black and red trajectories were recorded under a constant +70 mV transmembrane voltage. The normal ion channel conductance is reached after the appearance of a transient high-conductance (THC) state. (b) The average conductances of the normal channel and THC state. White is the average conductance of the normal ion channel, 70 ± 1.9 pS (based on 12 trajectories). Black is the average conductance of the THC state, 348 ± 135 pS (based on 52 THC states). (c) The zoom-in view of the THC state of the red trajectory in (a). It is apparent here that the THC state does not appear as a single spike. (d) The conductance distribution of the THC states. The mean conductance of the THC states is 310 pS from the distribution calculated from 52 trajectories. (e) The distribution of the open times of the THC state. The mean open time is 3.48 ms from the distribution calculated from 41 trajectories. (f) The distribution of the close times of the THC states. The mean close time is 4.47 ms from the distribution calculated from 52 trajectories. Therefore the average time of the THC state appearance in the membrane is 7.95 ms.

events and single-ion-channel electric recording trajectories, we have also calculated the distributions of open time and close time of the transient THC state [Figs. 3(e) and 3(f)], and the average lifetime of the observed THC states is found to be 8.0 ± 0.1 ms.

C. Correlated single-channel fluorescence microscopic imaging and single-channel electric recording to identify the hydrophilic water-pore pathway associated with the channel activation

To further identify that the THC state is due to the formation of a water-pore pathway in the membrane correlated with the ion channel activation, we have conducted a control experiment using Ca^{2+} flux imaging correlated with single-ion-channel current recordings [87]. Figures 4(a1)–4(a5) show the consecutive five imaging frames of the optical measurement, each with 3 ms exposure time, recorded during an ion channel activation event. A relatively brighter spot in the fluorescence imaging, indicating a high Ca^{2+} current and accumulation at the spot, appears [Fig. 4(b)] in correlation with the THC state appearance [Fig. 4(c)]. It is apparent that the electric conductance increases as the brighter imaging spot appears in the correlated recording, and the electric conductance drops back to the background level and the brighter spot disappears at the same time, showing a strong temporal correlation between the fluorescence imaging and electric conductance trajectories. The correlation between the increased fluorescence intensity and electric conductance suggests that the water-pore pathway formation in the lipid bilayer is the origin of the THC state appearance leading to the activation of the colicin Ia channel and following open-close activities. Furthermore, the images in Figs. 4(a2)–4(a4) cannot be due to a random leak of Ca^{2+} through the membrane or an already activated ion channel, because there is no observable imaging signal intensity above the background in Figs. 4(a1) and 4(a5) before and after the THC state occurrence event recorded simultaneously by single-ion-channel electric conductance detection (Fig. 4).

D. MD simulation analysis of voltage-sensor domain of ion channel protein translocation across the lipid bilayer membrane

To obtain a further molecular-level understanding of the charged peptide domain translocation across a lipid bilayer through a possible water pore associated with the THC state occurrence, we have conducted MD simulations with the C domain of colicin Ia under a transmembrane electric field. In recent years, MD simulations have emerged as a powerful approach to complement the experimental findings

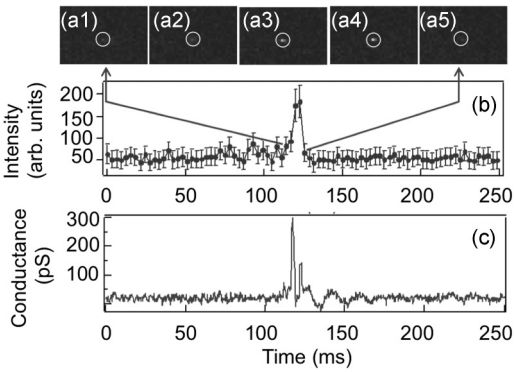

FIG. 4. Correlated fluorescence imaging and single-ion-channel current recording studies of the formation of the THC. (a) Consecutive five frames of Ca^{2+} imaging where the opening of the lipid bilayer is observed correlated with the ionic current measurement. The white circle shows the position of the brighter spot. The images were collected with 3 ms exposure time in an area of 100×33 binned pixels where each pixel in the image represents 2×4 pixels, and the binning of the pixels was done to keep the readout time less than the exposure time. (b) Correlated fluorescence intensity trajectory recorded by the fluorescence imaging. The error bar shows the standard deviation. (c) Correlated ion channel conductance trajectory recorded by ion channel voltage-clamping recording. The trajectory shows only the THC state but without significant on-off electric activity following, which benefits a clear optical imaging of the low-fluorescence background.

by providing detailed insight about translocation of bio- and inorganic molecules through lipid membranes [88–90]. We note that the aim of our MD simulation is to have a conceptual and qualitative understanding of the charged peptide diffusion across a lipid bilayer under a transmembrane voltage rather than exactly simulating the experimental results of colicin conformational dynamics in the time scale of milliseconds to minutes.

The umbrella conformation of the C domain [Fig. 1(b)] is used as the starting configuration of colicin Ia due to its reported lowest free energy amongst all the accessible conformations [78]. The DPhPC lipid bilayer model is constructed and simulated as discussed above. The MD simulation started with a 0.07 V/nm transmembrane electric field which is increased to 0.15 V/nm at 23 ns and maintained at that value throughout the rest of the simulation.

The simulation has evidenced that the translocation of the charged peptide domain across the hydrophobic lipid membrane is associated with a water-pore formation right at the peptide insertion site and across the lipid bilayer. Initially the water molecules penetrate stochastically the core of the hydrophobic bilayer to form a wirelike path [Figs. 5(a1) and 5(a2)]. As time passes the wirelike structure grows in size and expands to form a water-filled hydrophilic pore [Fig. 5(a3)] that provides a polar pathway for charged residues to translocate across the lipid membrane. We emphasize that the location of the water-pore formation is not random, but rather highly correlated to the site of the charged peptide residues in the membrane. We have run an adequate number of trajectories, and we have also run a number of trajectories using a different lipid bilayer, such as a 1,2-dipalmitoyl-*sn*-glycero-3-phosphocholine (DPPC)lipid bilayer (data not shown). In all the simulated trajectories, we observed that the water-pore is formed right under the peptide domains containing charged amino acids. In all cases the water wires appear from both

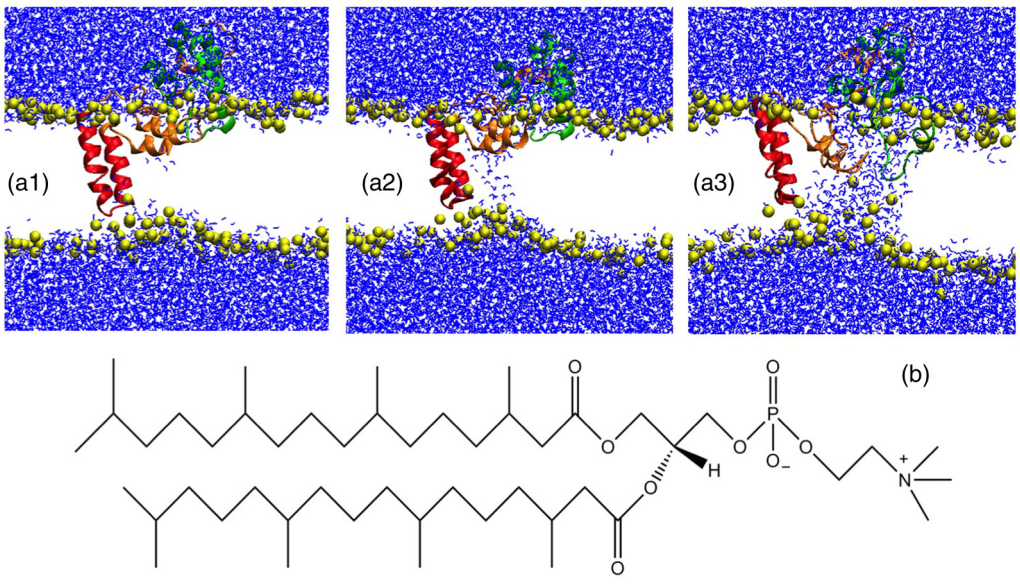

FIG. 5. (Color online) MD simulation snapshots of colicin Ia in the 1,2-diphytanoyl-*sn*-glycero-3-phosphocholine (DPhPC) lipid bilayer under a transmembrane electric field. (a) Formation of the water-filled pore pathway by the C domain driven under an electric field. Here we use only the phosphorus atom (yellow) to represent the lipid molecules. (a1) The deformation of the lipid bilayer starts under the charged peptide domains and water molecules from both sides of the bilayer start entering into the lipid bilayer (58 ns). (a2) The appearance of the water wire across the DPhPC bilayer (63 ns). (a3) The formation of a larger water-pore pathway across the lipid bilayer (76 ns). (b) Chemical structure of the DPhPC molecule.

sides of the lipid bilayer and they extend to join to form the water pore (Fig. 5). Several earlier studies reported that transmembrane segments containing charged residues, e.g., arginine or aspartic acid, induce deformation in the membrane either by dragging water molecules along with them or by snorkeling, thereby allowing water molecules to penetrate the bilayer [91–95]. The presence of extra protein content inside the bilayer further facilitates retaining of their hydration layer by charged residues [92]. Likewise, in our system, the fluctuation of helical hairpin segment (helices 8 and 9) inside the lipid bilayer likely induces some local deformation in the opposite side lipid leaflet through which interfacial waters seep deeper into the interfacial region while still maintaining the structural integrity of the lipid bilayer. This deformation is further enhanced as the charged voltage-sensor domain drags more water molecules with it in retaining its energetically accessible hydration. At the later stage, lipid head groups reorient themselves sparsely to margin the water pore thus stabilizing the water pore [81].

The characteristics of the lipid bilayer, i.e., the thickness and the density of lipid appear to be highly correlated with the water-pore formation. We have calculated the thickness of the lipid bilayer during the formation of the water-pore pathway across the membrane using GRIDMAT-MD [96] and results are shown in Fig. 6(a). The thinning of the lipid bilayer near charged peptide residues is first observed after 58 ns, and continues throughout the rest of the simulation as the water pore increases in size [Fig. 6(a)]. Furthermore, the densities of DPhPC molecules and water molecules in the membrane normal direction also show significant variations during the water-pore pathway formation [Figs. 6(b1) and 6(b2)]. Before the water wire appears, no water molecule is present in the hydrophobic core region between the two DPhPC leaflets. When the water wire occurs, the density of water molecules dramatically increases with time. This corresponds to the formation of the water-filled pore pathway. The density of DPhPC shows the inverse behavior compared to the water molecule density [Fig. 6(b2)]. We note that as the local region becomes thinner to form the water-pore pathway, the other area around the water-pore pathway region shows an increasing or unchanged thickness of the DPhPC membrane as shown by the green curve in Fig. 6(b2). The thickness changes are consistent with the increasing entropies of water and the DPhPC molecules [97]. We stress here that our MD simulation finding only qualitatively supports our experimental findings. To make a quantitative or semiquantitative correspondence with the experimental results, we need long simulation runs to calculate the pore formation dynamics and structural calculation, which is technically beyond the scope of this work.

To rule out electroporation, i.e., the possibility of water-pore pathway formation in a lipid bilayer by an external electric field alone [98,99], we have used significantly lower electric fields for our simulation than that of the previously reported minimum strength required for electroporation [100–103], and the water-pore pathway is not formed at a random location but rather a highly specific location right under the charged residues of the colicin Ia (Figs. 5 and 6). To check further, we ran MD simulation on the bare DPhPC bilayer with a 0.15 V/nm electric field. We did not notice any signature of water-pore formation even after 125 ns [81]. The phenomenon of electroporation at such a low electric field may take hundreds of nanoseconds to initiate. As we see that water-pore formation starts at ∼50 ns with such a low electric field in our system, we can certainly rule out the possibility of

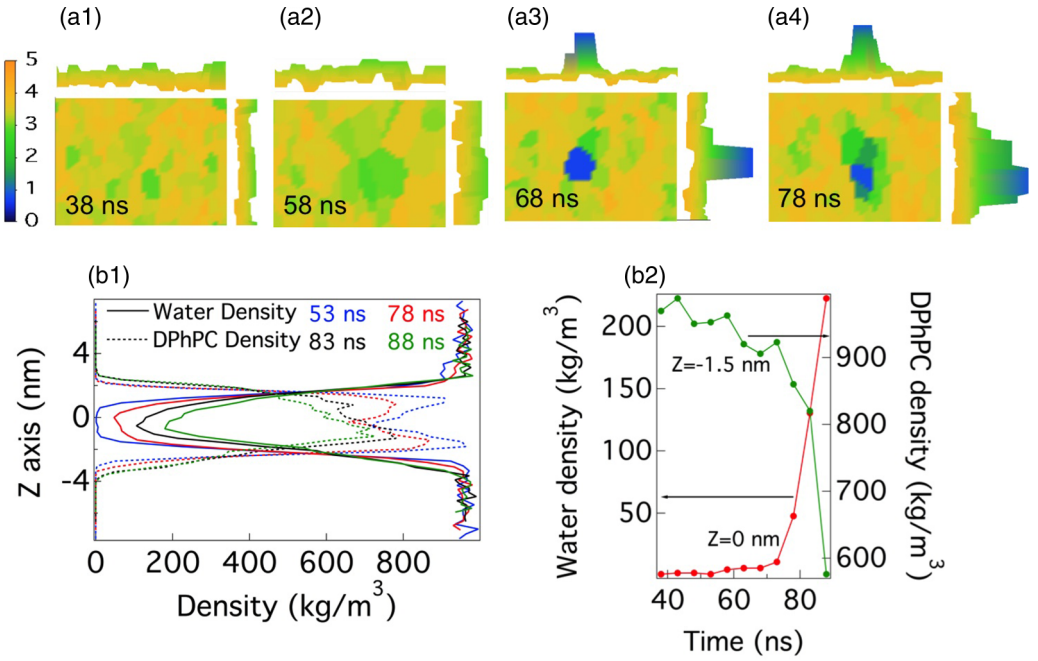

FIG. 6. (Color online) MD simulation of colicin Ia in the DPhPC lipid bilayer under a transmambrane electric field. (a) The thickness variation of the lipid bilayer (in nanometers) with time during water-pore formation. (b1) Density of the water molecules and DPhPC molecules in slabs along the Z axis of the simulation box (membrane normal direction). (b2) Density variation of water molecules of a specific slab with center located at $Z = 0$ nm and density variation of DPhPC molecules of a specific slab located at $Z = -1.5$ nm.

electroporation when colicin is inserted in the lipid bilayer. In a separate MD run, we switched off the electric field after a sufficiently large water pore is formed (78 ns here) to observe whether this leads to membrane reconstruction. We did not run long enough simulations to observe the complete membrane resealing; however, we did observe a decrease in water-pore size [81]. It is to be noted that the membrane reconstruction process in our present system may take a much longer time compared to previous reports [104] as the water pore gets stabilized due to the interaction of counterions with the lipid head group. Additionally, we also checked whether peptide-membrane interaction in the absence of any transmembrane electric field could initiate the water-pore formation. For that purpose, we ran MD simulation without any transmembrane electric field while the C domain of colicin Ia is inserted in the lipid membrane. Even after 80 ns of MD run, we did not see any signature of water-wire or water-pore formation [81]. Although cationic peptides are found to be responsible for membrane disruption by interacting specifically with negatively charged lipid membranes at moderate to high protein to lipid molar ratio [105], in our system, the zwitterionic nature of the DPhPC bilayer with very low protein to lipid molar ratio could be the reason for no initiation of water-pore formation without a transmembrane electric field. Therefore, based on all of the control experimental and computational results, we attribute the formation of the water pore to be uniquely induced by the polypeptide, especially the charged voltage-sensor residues of colicin Ia under the transmembrane electric field.

In our experimental measurements discussed above, it takes hundreds of milliseconds to minutes for the formation of the water-filled pathway before the colicin polypeptide voltage-sensor segment diffuses across the lipid membrane. However, in our MD simulation the applied electric field is 3.5 to 7.5 times higher than in the previous reports [98,99]. The reason behind this is to initiate the water-pore formation on a shorter time scale while still showing essentially the same characteristics. It is expected that the water-pore formation in a lower electric field would be much slower in our MD simulation but would still occur. Nevertheless, the essential physical nature of the water-pore pathway formation induced by the voltage-sensor domain of the colicin Ia is characterized in our MD simulation, suggesting that the charged residue regions of colicin Ia promote the deformation of the lipid bilayer, thereby acting as a precursor for the water-filled hydrophilic pathway formation. The highly specific and nonrandom location of the water pore right under the voltage-sensor peptide domain further corroborates this finding.

Overall, our MD simulation serves as a qualitative or semiquantitative control on the interpretation of our experimental results, which suggests that (1) there are early events that lead to a propensity of water-pore formation; (2) the water-pore formation is completely nonrandom but right at the site in the lipid membrane where the charged peptide domain resides; and (3) the charged peptide domain diffuses across the membrane through the hydrophilic water-pore. Our MD simulation in particular or a typical MD simulation may not be able to observe a stable water pore in its equilibrium state, as it is most likely that the charged peptide diffusing across a transient water pore is a highly dynamic process in nature. We note that we have run MD simulations with the same starting structure of colicin Ia inserted in the DPhPC bilayer but without an applied transmembrane electric field. We did not observe any signature of water-pore formation even after 80 ns, whereas water wire starts forming under the applied transmembrane field at ∼50 ns. To make a quantitative or semiquantitative correspondence with the experimental results, namely, equilibrium open-close dynamics, there is a need for much longer simulation runs, which are beyond the scope of this work.

E. Model of voltage-sensor domain transmembrane motions

The model for the formation of the colicin Ia channel in a lipid bilayer was first proposed by Kienker *et al.* [33], describing (1) adsorption of the C domain to the membrane; (2) orientation of the α-helices 8–9 and their insertion into the membrane; (3) formation of the ion channel through translocation of the charged voltage-sensor helices 2–5 across the membrane driven under a transmembrane voltage. However, thus far, neither this model nor apparently any other reported works have identified or described the specific mechanism and dynamics of the channel open-close conformational motions and the translocation of helices 2–5 across the membrane. According to the conventional mechanism, channel open and close events are mostly regulated by the transmembrane voltage. Also, the charged polypeptide domain presumably involves solvation and desolvation as it moves from one hydrophilic side to the other hydrophilic side, crossing the hydrophobic core of the membrane. However, the question remains how a charged polypeptide can cross the energy barrier to move inside the hydrophobic core of the membrane. Because it is well known that there is not enough energy available for such desolvation and interaction between the hydrophilic and charged polypeptide domains with the hydrophobic core of the lipid tiles in the membrane, even under the driving of the transmembrane voltage. Based on our experimental and MD simulation results, we are now able to provide additional insight about the colicin Ia channel open-close events and water-filled pore formation pathway, to identify how the charged domain of colicin Ia (helices 2–5) diffuses, crossing the hydrophobic core of the lipid bilayer to form the four-subunit ion channel. We propose a modified model for translocation of the colicin Ia α-helices 2–5 across the membrane (Fig. 7): (1) After being introduced into the cis solution, the colicin Ia diffuses randomly before it comes onto and gets adsorbed on the lipid bilayer [Fig. 7(a)]. (2) Then the hydrophobic hairpin inserts itself into the lipid bilayer, generating the umbrella structure [Fig. 7(b)]. (3) Driven by the external transmembrane electric field, charged residues of colicin Ia induce a deformation in the lipid bilayer, directing the water to form conical intrusions into the lipid bilayer, starting as a water wire across the membrane [Fig. 7(c)]. (4) The water intrusions, along with the solvation layer of the charged polypeptide segment, form a larger hydrophilic pore that provides a polar and aqueous pathway for the charged residues of colicin Ia to diffuse across the hydrophobic lipid bilayer under the driving force of the 70 mV transmembrane voltage [Fig. 7(d)]. (5) In the following step of the ion channel activation, the pore pathway closes while having four helices in the lipid

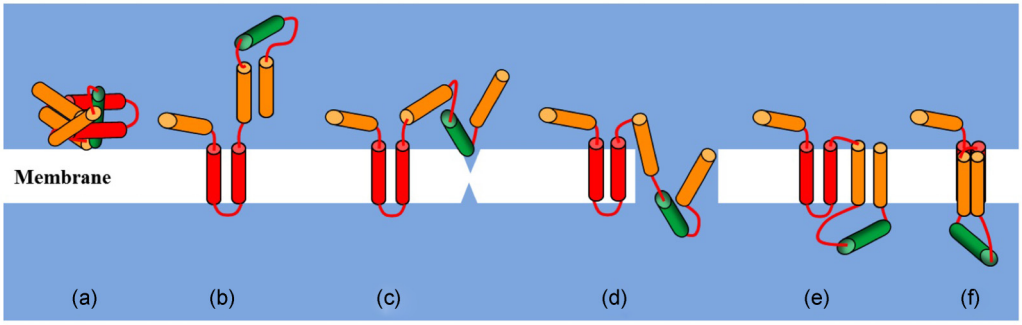

FIG. 7. (Color online) The model for the diffusional translocation of the α-helices 2–5 (green) across the hydrophobic lipid bilayer [color scheme as in Fig. 1(c)]. (a) Adsorption of the colicin Ia onto the lipid bilayer. (b) The umbrella structure of colicin Ia. The hydrophobic (red) segment has inserted into the lipid bilayer. (c) Formation of water wire inside the lipid bilayer. (d) Formation of a large hydrophilic water-pore pathway and translocation of the helices 2–5 of the colicin Ia across the lipid bilayer. (e) After translocation, the water pore disappears due to a spontaneous membrane self-repair, and the helices 1, 6, 7, 8, and 9 are positioned inside the lipid bilayer. (f) The formation and activation of the normal ion channel.

bilayer and the α-helices 2–5 in the trans side of the lipid bilayer [Fig. 7(e)]. (6) In the final step, the four helices form the channel of colicin Ia [Fig. 7(f)], which produces open and closed states mostly due to the ion channel's conformational fluctuations driven by local thermal fluctuations. Nevertheless, the core element of the energetics and dynamics of the ion channel activation is the solvation of the colicin polypeptide domain by hydrophilic water and hydrophobic lipid molecules under an external transmembrane voltage [100–103]. Overall, according to our mechanism, the charged polypeptide domain actually does not involve a significant solvation-desolvation dynamics but rather diffuses across the membrane through an essentially hydrophilic pathway; although the solvation fluctuation plays a significant role in the water-filled pore formation across the membrane under the transmembrane voltage.

The mechanism of the voltage-sensor domain translocation across the lipid membrane is inhomogeneous and complex, and our proposed water-pore pathway mechanism does not necessarily exclude the conventional mechanisms [7,13,19,20,106,107]. Although we have observed a 40% $\pm$ 10% probability of THC state occurrence in the recorded active-ion-channel activation events, there are portions of THC state occurrences that are not followed by a measurable active-ion-channel formation. Furthermore, certain portion of ion channel formation events occurs without any observable THC state. Possible reasons might be the following: (1) the voltage-sensor domain diffuses across the lipid membrane solely as transmembrane voltage driven, consistent with the conventional mechanism; (2) the hydrophilic water-pore pathway existence is too transient to be detected by either the fluorescence imaging or the electrophysiological conductance recording; (3) the water-pore pathway associated with the voltage-sensor domain diffusion is transient and fluctuating together with peptide solvation fluctuations, and in the course of the polypeptide domain relocation across the membrane, the hydrophilic water-pore pathway is never fully formed at any time but is formed on average in time. Definitely, additional investigations are needed to resolve the ion channel formation and activation events without a measureable THC state occurrence, and the complexity and inhomogeneity of the molecular dynamics must be considered in the overall process of voltage-sensor domain translocation across the lipid membrane under a constant transmembrane voltage. Furthermore, the membrane local environment is definitely even more complex and inhomogeneous, which most likely involves more complex mechanisms with multiple pathways. However, such further studies are beyond the scope of this reported work. Nevertheless, the water-pore pathway formation mechanism proposed in this work is significant and important in the case of colicin ion channel formation, and the mechanism elucidates the profound physical nature of the voltage-sensor polypeptide domain motions and voltage-gated ion channel activities under a transmembrane voltage.

IV. CONCLUSIONS

We have applied a combined fluorescence imaging and electric conductance recording approach, correlated with computational molecular dynamics simulations, to study the mechanism and dynamics of colicin Ia charged domain translocation across the lipid bilayer in the activation of the colicin ion channel. Our results reveal a mechanism in which the activation of the ion channel is due to voltage-sensor domain diffusion across the lipid bilayer membrane under a transmembrane voltage. We have identified a significant probability that the colicin ion channel activation events are associated with a high-conductance state resulting from the formation of a water pore in the lipid bilayer as large as $\sim$15 Å diameter. This experimental result is supported and further identified from our molecular dynamics simulations. The water-pore pathway provides an energetically favorable polar pathway for the charged voltage-sensor α-helices to cross the lipid bilayer in order to form the activated channel configuration. The most significant result of our MD simulation is that the location of the water-pore formation in the membrane is always nonrandom and right under the voltage-sensor peptide domain. Ultimately, charged peptide solvation energetics and dynamics play a critical role in the water-filled pathway formation. Here we are able to shed light on the

fundamental translocation mechanism of a voltage-sensor charged polypeptide domain under an external electric field: the charged polypeptide domain facilitates the formation of a water-pore pathway in the membrane and diffuses through that hydrophilic pathway across the membrane, thereby forming the activated ion channel. Although the results presented here are based on the study of colicin Ia as a model system, the knowledge obtained here can have significant implications for understanding other voltage-gated ion channel activation mechanisms and dynamics in living cells.

ACKNOWLEDGMENTS

The colicin Ia we used for this study has only the C domain and was purified, mutated, fluorescein labeled, and biotinylated by Professor A. Finkelstein and co-workers in Albert Einstein College of Medicine, New York. This work is supported by Ohio Eminent Scholar Endowment Fund and NIH National Institute of General Medical Sciences (Grant No. 5 R01 GM098089). We acknowledge our usage of the computational facility of the Ohio Supercomputer Center, Columbus, Ohio.

[1] B. Hille, *Ionic Channels of Excitable Membranes* (Sinauer Associates, Sunderland, MA, 1984).
[2] W. A. Catterall, Science **242**, 50 (1988).
[3] H. R. Leuchtag, *Voltage-Sensitive Ion Channels: Biophysics of Molecular Excitability* (Springer, Dordrecht, The Netherlands, 2008).
[4] S. L. Slatin, X. Qiu, K. S. Jakes, and A. Finkelstein, Nature (London) **371**, 158 (1994).
[5] X. Q. Qiu, K. S. Jakes, A. Finkelstein, and S. L. Slatin, J. Biol. Chem. **269**, 7483 (1994).
[6] X. Q. Qiu, K. S. Jakes, P. K. Kienker, A. Finkelstein, and S. L. Slatin, J. Gen. Physiol. **107**, 313 (1996).
[7] Y. Jiang, V. Ruta, J. Chen, A. Lee, and R. MacKinnon, Nature (London) **423**, 42 (2003).
[8] B. Chanda and F. Bezanilla, J. Gen. Physiol. **120**, 629 (2002).
[9] W. Treptow, B. Maigret, C. Chipot, and M. Tarek, Biophys. J. **87**, 2365 (2004).
[10] H. Vogel, L. Nilsson, R. Rigler, S. Meder, G. Boheim, W. Beck, H.-H. Kurth, and G. Jung, Eur. J. Biochem. **212**, 305 (1993).
[11] S. Dorairaj and T. W. Allen, Proc. Natl. Acad. Sci. USA **104**, 4943 (2007).
[12] M. Grabe, H. Lecar, Y. N. Jan, and L. Y. Jan, Proc. Natl. Acad. Sci. USA **101**, 17640 (2004).
[13] T. Hessa, H. Kim, K. Bihlmaier, C. Lundin, J. Boekel, H. Andersson, I. Nilsson, S. H. White, and G. von Heijne, Nature (London) **433**, 377 (2005).
[14] L. Hong, M. M. Pathak, I. H. Kim, D. Ta, and F. Tombola, Neuron **77**, 274 (2013).
[15] K. Matsuzaki, O. Murase, N. Fujii, and K. Miyajima, Biochemistry **34**, 6521 (1995).
[16] K. Bhattacharyya, Chem. Commun. 2848 (2008).
[17] D. K. Das, T. Mondal, U. Mandal, and K. Bhattacharyya, ChemPhysChem **12**, 814 (2011).
[18] U. Anand, C. Jash, and S. Mukherjee, Phys. Chem. Chem. Phys. **13**, 20418 (2011).
[19] G. Yellen, Nature (London) **419**, 35 (2002).
[20] G. Yellen, Q. Rev. Biophys. **31**, 239 (1998).
[21] C. M. Armstrong and B. Hille, Neuron **20**, 371 (1998).
[22] J. Konisky, Annu. Rev. Microbiol. **36**, 125 (1982).
[23] P. K. Kienker, K. S. Jakes, and A. Finkelstein, J. Gen. Physiol. **116**, 587 (2000).
[24] K. S. Jakes, P. K. Kienker, and A. Finkelstein, Q. Rev. Biophys. **32**, 189 (1999).
[25] P. Elkins, A. Bunker, W. A. Cramer, and C. V. Stauffacher, Structure **5**, 443 (1997).
[26] M. Wiener, D. Freymann, P. Ghosh, and R. M. Stroud, Nature (London) **385**, 461 (1997).
[27] S. L. Slatin and P. K. Kienker, *Colicin channels and protein translocation. Parallels with diphtheria toxin, in* Pore Forming Peptides and Protein Toxins, edited by G. Menestrina (Taylor and Francis, London, 2003), p. 102.
[28] W. A. Cramer, J. B. Heymann, S. L. Schendel, B. N. Deriy, F. S. Cohen, P. A. Elkins, and C. V. Stauffacher, Annu. Rev. Biophys. Biomol. Struct. **24**, 611 (1995).
[29] R. A. Nogueira and W. A. Varanda, J. Membrane Biol. **105**, 143 (1988).
[30] P. Ghosh, S. F. Mel, and R. M. Stroud, J. Membrane Biol. **134**, 85 (1993).
[31] R. Stroud, Curr. Opin. Struct. Biol. **5**, 514 (1995).
[32] W. Luo, X. Yao, and M. Hong, J. Am. Chem. Soc. **127**, 6402 (2005).
[33] P. K. Kienker, X. Qiu, S. L. Slatin, A. Finkelstein, and K. S. Jakes, J. Membrane Biol. **157**, 27 (1997).
[34] N. Yang, A. L. George, and R. Horn, Neuron **16**, 113 (1996).
[35] F. Tombola, M. Pathak, and E. Y. Isacoff, Annu. Rev. Cell Dev. Biol. **22**, 23 (2006).
[36] S. P. Rajapaksha, X. Wang, and H. P. Lu, Anal. Chem. **85**, 8951 (2013).
[37] G. S. Harms, G. Orr, M. Montal, B. D. Thrall, S. D. Colson, and H. P. Lu, Biophys. J. **85**, 1826 (2003).
[38] H. P. Lu, L. Y. Xun, and X. S. Xie, Science **282**, 1877 (1998).
[39] G. Harms, G. Orr, and H. P. Lu, Appl. Phys. Lett. **84**, 1792 (2004).
[40] www.gromacs.org
[41] B. Hess, C. Kutzner, D. van der Spoel, and E. Lindahl, J. Chem. Theory Comput. **4**, 435 (2008).
[42] D. van der Spoel, E. Lindahl, B. Hess, G. Groenhof, A. E. Mark, and H. J. C. Berendsen, J. Comput. Chem. **26**, 1701 (2005).
[43] E. Lindahl, B. Hess, and D. van der Spoel, J. Mol. Model. **7**, 306 (2001).
[44] H. J. C. Berendsen, D. van der Spoel, and R. Van Drunen, Comput. Phys. Commun. **91**, 43 (1995).
[45] J. Hermans, H. J. C. Berendsen, W. F. Van Gunsteren, and J. P. M. Postma, Biopolymers **23**, 1513 (1984).
[46] O. Berger, O. Edholm, and F. Jahnig, Biophys. J. **72**, 2002 (1997).
[47] D. P. Tieleman and H. J. C. Berendsen, J. Chem. Phys. **105**, 4871 (1996).
[48] http://lipidbook.bioch.ox.ac.uk/package/show/id/20.html
[49] C. Kandt, W. L. Ash, and D. P. Tieleman, Methods **41**, 475 (2007).
[50] H. J. C. Berendsen, J. P. M. Postma, W. F. van Gunsteren, and J. Hermans, Intermol. Forces **14**, 331 (1981).

[51] S. A. Nosé, J. Chem. Phys. **81**, 511 (1984).
[52] W. G. Hoover, Phys. Rev. A **31**, 1695 (1985).
[53] M. Parrinello and A. Rahman, J. Appl. Phys. **52**, 7182 (1981).
[54] S. Nosé and M. L. Klein, Mol. Phys. **50**, 1055 (1983).
[55] B. Hess, H. Bekker, H. J. C. Berendsen, and J. G. E. M. Fraaije, J. Comput. Chem. **18**, 1463 (1997).
[56] T. Darden, D. York, and L. Pedersen, J. Chem. Phys. **98**, 10089 (1993).
[57] W. Humphrey, A. Dalke, and K. Schulten, J. Mol. Graphics **14**, 33 (1996).
[58] F. Ryttsén, C. Farre, C. Brennan, S. G. Weber, K. Jardemark, D. T. Chiu, and O. Orwar, Biophys. J. **79**, 1993 (2000).
[59] H. P. Lu, Acc. Chem. Res. **38**, 557 (2005).
[60] H. P. Lu, Methods Cell Biol. **90**, 435 (2008).
[61] T. Ide, M. Hirano, and Y. Takeuchi, *Ion Channels, in Single Molecule Dynamics in Life Science*, edited by T. Yanagida and Y. Ishii (Wiley-VCH Verlag GmbH & Co. KGaA, Weinheim, Germany, 2008), Chap. 4.
[62] M. Andersson, J. A. Freites, D. J. Tobias, and S. H. White, J. Phys. Chem. B **115**, 8732 (2011).
[63] D. Krepkiy, M. Mihailescu, J. A. Freites, E. V. Schow, D. L. Worcester, K. Gawrisch, D. J. Tobias, S. H. White, and K. J. Swartz, Nature (London) **462**, 473 (2009).
[64] V. Yarov-Yarovoy, P. G. DeCaen, R. E. Westenbroek, C.-Y. Pan, T. Scheuer, D. Baker, and W. A. Catterall, Proc. Natl. Acad. Sci. USA **109**, E93 (2012).
[65] E. C. McCusker, C. Bagnéris, C. E. Naylor, A. R. Cole, N. D'Avanzo, C. G. Nichols, and B. A. Wallace, Nat. Commun. **3**, 1102 (2012).
[66] J. C. Gumbart, I. Teo, B. Roux, and K. Schulten, J. Am. Chem. Soc. **135**, 2291 (2013).
[67] F. Khalili-Araghi, E. Tajkhorshid, B. Roux, and K. Schulten, Biophys. J. **102**, 258 (2012).
[68] M. O. Jensen, V. Jogini, D. W. Borhani, A. E. Leffler, R. O. Dror, and D. E. Shaw, Science **336**, 229 (2012).
[69] Z. Lai, K. Zhang, and J. Wang, Phys. Chem. Chem. Phys. **16**, 6486 (2014).
[70] X. Zheng and J. Wang, PLoS Comput Biol **11**, e1004212 (2015).
[71] T. B. Woolf and B. Roux, Proc. Nalt. Acad. Sci. USA **91**, 11631 (1994).
[72] L. Saiz and M. L. Klein, Acc. Chem. Res. **35**, 482 (2002).
[73] M. B. Ulmschneider, J. P. Ulmschneider, N. Schiller, B. A. Wallace, G. von Heijne, and S. H. White, Nat. Commun. **5**, 4863 (2014).
[74] W. L. Ash, M. R. Zlomislic, E. O. Oloo, and D. P. Tieleman, Biochim. Biophys. Acta, Biomembr. **1666**, 158 (2004).
[75] L. R. Forrest and M. S. Sansom, Curr. Opin. Struct. Biol. **10**, 174 (2000).
[76] S. K. Kandasamy and R. G. Larson, Biophys. J. **90**, 2326 (2006).
[77] S. S. Deol, P. J. Bond, C. Domene, and M. S. P. Sansom, Biophys. J. **87**, 3737 (2004).
[78] L. Prieto and T. Lazaridis, Proteins **79**, 126 (2011).
[79] D. Chandler, *Introduction to Modern Statistical Mechanics* (Oxford University Press: New York,1987).
[80] A. A. Aleksandrov and J. R. Riordan, FEBS Lett. **431**, 97 (1998).
[81] See Supplemental Material at http://link.aps.org/supplemental/10.1103/PhysRevE.92.052719 for the analysis of conductance trajectories at 50 mV and 100 mV transmembrane voltage, simulation snapshots of the solvated DPhPC bilayer under a transmembrane electric field, colicin Ia in a DPhPC bilayer after the transmembrane electric field is switched off, colicin Ia in a DPhPC bilayer without any transmembrane electric field, and the movies generated from the simulation snapshots of colicin Ia in a DPhPC bilayer under a transmembrane electric field.
[82] M. L. Scalley and D. Baker, Proc. Natl. Acad. Sci. USA **94**, 10636 (1997).
[83] T.-L. Kuo, S. Garcia-Manyes, J. Li, I. Barel, H. Lu, B. J. Berne, M. Urbakh, J. Klafter, and J. M. Fernandez, Proc. Natl. Acad. Sci. USA **107**, 11336 (2010).
[84] H. Frauenfelder, S. G. Sligar, and P. G. Wolynes, Science **254**, 1598 (1991).
[85] H. Frauenfelder and P. G. Wolynes, Phys. Today **47**(2), 58 (1994).
[86] O. V. Krasilnikov, J. B. Da Cruz, L. N. Yuldasheva, W. A. Varanda, and R. A. Nogueira, J. Membrane Biol. **161**, 83 (1998).
[87] L. M. Harriss, B. Cronin, J. R. Thompson, and M. I. Wallace, J. Am. Chem. Soc. **133**, 14507 (2011).
[88] W. F. D. Bennett and D. P. Tieleman, Acc. Chem. Res. **47**, 2244 (2014).
[89] J. Lin and A. Alexander-Katz, ACS Nano **7**, 10799 (2013).
[90] B. Song, H. Yuan, S. V. Pham, J. J. Cynthia, and S. Murad, Langmuir **28**, 16989 (2012).
[91] J. Gumbert, C. Chipot, and K. Schulten, Proc. Natl. Acad. Sci. USA **108**, 3596 (2011).
[92] A. C. V. Johansson, and E. Lindahl, Proc. Natl. Acad. Sci. USA **106**, 15684 (2009).
[93] N. A. Berglund, T. J. Piggot, D. Jefferies, R. B. Sessions, P. J. Bond, and S. Khalid, PLoS Comput Biol **11**, e1004180 (2015).
[94] A. C. V. Johansson and E. Lindahl, Biophys. J. **91**, 4450 (2006).
[95] E. Strandberg and J. A. Killian, FEBS Lett. **544**, 69 (2003).
[96] W. J. Allen, J. A. Lemkul, and D. R. Bevan, J. Comput. Chem. **30**, 1952 (2008).
[97] J. A. Freites, D. J. Tobias, G. von Heijne, and S. H. White, Proc. Natl. Acad. Sci. USA **102**, 15059 (2005).
[98] D. P. Tieleman, H. Leontiadou, A. E. Mark, and S. J. Marrink, J. Am. Chem. Soc. **125**, 6382 (2003).
[99] D. P. Tieleman, BMC Biochem. **5**, 10 (2004).
[100] L. Wang, R. A. Friesner, and B. J. Berne, Faraday Discuss. **146**, 247 (2010).
[101] J. E. Ladbury, Chem. Biol. **3**, 973 (1996).
[102] S. K. Buchanan, P. Lukacik, S. Grizot, R. Ghirlando, M. M. Ali, T. J. Barnard, K. S. Jakes, P. K. Kienker, and L. Esser, EMBO J. **26**, 2594 (2007).
[103] J. Kyte and R. F. Doolittle, J. Mol. Biol. **157**, 105 (1982).
[104] M. Tarek, Biophys. J. **88**, 4045 (2005).
[105] L. Chen, X. Li, L. Gao, and W. Fang, J. Phys. Chem. B **119**, 850 (2015).
[106] Y. Jiang, A. Lee, J. Chen, V. Ruta, M. Cadene, B. T. Chait, and R. MacKinnon, Nature (London) **423**, 33 (2003).
[107] T. Hessa, S. H. White, and G. von Heijne, Science **307**, 1427 (2005).